

# A mechanism for preferential H<sub>2</sub>O leakage from fluid inclusions in quartz, based on TEM observations

Ronald J. Bakker, and J. Ben H. Jansen\*

Department of Geochemistry, Institute for Earth Sciences, Utrecht University, P.O.Box 80.021, NL-3508 TA Utrecht, The Netherlands

Received: May 5, 1993 / Accepted October 15, 1993

**Abstract.** Preferential leakage of H<sub>2</sub>O from fluid inclusions containing multiple gas components has been suspected in natural metamorphic rocks and has been demonstrated experimentally for synthetic H<sub>2</sub>O-CO<sub>2</sub>-rich inclusions in natural quartz. Knowledge of the physical and chemical characteristics of the leakage mechanism, which may be very complex, increases the value of natural fluid inclusions to metamorphic geology. It is proposed that crystal defects play a major role in non-decrepitative preferential H<sub>2</sub>O leakage through quartz, and remain effective during metamorphism. Inclusions with either an internal overpressure or underpressure produce strain in the adjacent quartz crystal via the nucleation of many dislocations and planar defects (like Dauphiné twin boundaries). These defects allow preferential loss of H<sub>2</sub>O from H<sub>2</sub>O-CO<sub>2</sub>-rich inclusions at supercritical conditions. The transport capacity of this leakage mechanism is enhanced by nucleation of small bubbles on defect structures. The nucleation of these bubbles seems to be a recovery process in strained crystals. Solubility gradients of quartz in water in a crystal with internally underpressurized inclusions may result in optical visible implosion halos in a three dimensional spatial arrangement, caused by the growth of small bubbles at the expense of the larger original fluid inclusion. Natural fluid inclusions from Naxos (Greece) are always associated with numerous interlinked dislocations. These dislocations may have been produced by plastic deformation or by crystal growth related processes (e.g. crack healing). The presence of small bubbles on these dislocations indicates that a similar leakage mechanism for H<sub>2</sub>O must have occurred in these rocks.

## Introduction

Natural aqueous fluid inclusions in metamorphic rock may have preferentially leaked H<sub>2</sub>O. Water leakage may

be implied from fluid inclusions in metamorphic rocks which experienced *P-T* conditions which do not correspond with the specific isochore of the trapped fluid at peak metamorphic conditions. Selective H<sub>2</sub>O leakage is not necessarily uniform within both grains and single trails, and some H<sub>2</sub>O-rich inclusions may not have leaked at all, which indicate that the mechanism is complex (e.g. Roedder 1984).

Synthetic H<sub>2</sub>O-CO<sub>2</sub> fluid inclusions have been produced in quartz by Bakker and Jansen (1990, 1991). They showed that non-decrepitative H<sub>2</sub>O leakage may occur during re-equilibration at conditions differing from the original conditions of entrapment. Inclusions were synthesized through crack-healing processes in gem-quality Brazilian quartz. The re-equilibration experiments mimic the changing *P-T* conditions experienced by rocks, following real metamorphic *P-T*-paths. Non-uniform preferential leakage of H<sub>2</sub>O occurred, without evidence of decrepitation or inclusion-volume adjustments, during re-equilibration experiments which simulated isothermal compression and isothermal decompression at 835 K. It is not possible to identify routes for leakage using optical microscopy. Small open cracks or channels connected with inclusions appear to be absent.

Crystal defects in natural quartz have been studied using Transmission Electron Microscopy (TEM) since investigations suggested that plastic deformation in quartz is accommodated by dislocation movement (e.g. McLaren and Phakey 1965; Doukhan and Trepied 1985). To explain the hydrolytic weakening phenomenon in natural and synthetic quartz, water-related point defect bulk diffusion through the crystal and water enhanced mobility of dislocations were intensively studied. The main argument for water-related point defect bulk diffusion in synthetic quartz and natural amethyst is the formation of small bubbles during annealing experiments (McLaren et al. 1983; Gerretsen et al. 1989). A similar phenomenon has already been described by Wolff (1845) and Ferguson (1914), who observed that natural quartz became milky white after annealing, due to the formation of numerous very small fluid inclusions. Water-related point defects consist mainly of 4(H)<sub>i</sub> substitutes, H<sub>2</sub>O interstitials, and

Correspondence to: R.J. Bakker, CREGU, BP 23, F-54501 Vandœuvre-les-Nancy Cedex, France

\* Present address: BOWAGEMI BV, Prinses Beatrixlaan 20, NL-3972 AN Driebergen, The Netherlands

hydrogen/alkali exchange (e.g. McLaren et al. 1983; Kronenberg et al. 1986). Their solubility in quartz as a function of temperature and pressure has been theoretically calculated (Paterson 1986; Doukhan and Paterson 1986) to be less than  $100\text{H}/10^6\text{Si}$ , even at high temperature and pressure. This was confirmed by infrared absorption measurements in experimentally annealed natural and synthetic quartz (Aines et al. 1984; Rovetta et al. 1986; Gerretsen et al. 1989; Cordier and Doukhan 1989). The measured solubility and bulk diffusivity of water-related point defects, as reviewed by FitzGerald et al. (1991), is too low for significant penetration in single crystals and noticeable leakage of  $\text{H}_2\text{O}$  during our re-equilibration experiments. Although theoretical considerations indicate that pipe diffusion may be dominant over bulk diffusion (FitzGerald et al. 1991; Bakker and Jansen 1991), no measurements have been made in quartz. Diffusion of water-related species along dislocation cores were investigated only in feldspars by Yund et al. (1981).

In this study, it is proposed that the mechanism responsible for non-decrepitative preferential  $\text{H}_2\text{O}$  leakage from fluid inclusions is strongly related to diffusion, solution, and precipitation processes associated with dislocations and planar defects, which can be identified with TEM. Dislocations and planar defects are assumed to play a major role in molecular  $\text{H}_2\text{O}$  diffusion through quartz crystals. Furthermore, similar microstructures have been observed in the quartz around natural fluid inclusions in samples from the metamorphic complex of Naxos (Greece), which indicate that similar processes may occur despite the relatively short duration of experiments.

Although preferential  $\text{H}_2\text{O}$  leakage may seem to reduce the credibility of fluid inclusion studies to metamorphic geology, as leakage leads to density and composition changes, information about the mechanism of leakage of natural inclusions may enable the original inclusion density and composition to be reconstructed. Furthermore, details of the uplift path may be deduced from inclusions that have leaked, if leakage mechanism are restricted to particular conditions.

## Experimental sample preparation and results

Here we summarize the experimental procedure and results of experiments performed by Bakker and Jansen (1991) to investigate modifications of fluid inclusions.  $\text{H}_2\text{O}$ - $\text{CO}_2$ -rich fluid inclusions were synthesized in a 4 mm diameter cylindrical quartz core, which was drilled from a crack- and inclusion-free natural Brazilian quartz crystal. The experimental method which is described in detail by Sterner and Bodnar (1984) and Bakker and Jansen (1991), is based on the fact that healed cracks are always marked with numerous fluid inclusions. During the experimental runs,  $\text{CO}_2$  was introduced as a product of the explosive decomposition of silver-oxalate at 413 K. Before decomposition, part of the silver-oxalate may be dissolved in water, which may influence the miscibility properties of the fluid. However, its solubility in water is negligible. Crack healing was performed at 835 K and 200 MPa confining pressure (initial experiment E421 in Fig. 1) exerted by a gas mixture of  $X_{\text{CO}_2} \approx 0.2$  and  $X_{\text{H}_2\text{O}} \approx 0.8$  in an arc-welded gold capsule. The homogenization temperatures of the fluid in synthetic inclusions reflect one density which is in accordance with the density at experimental

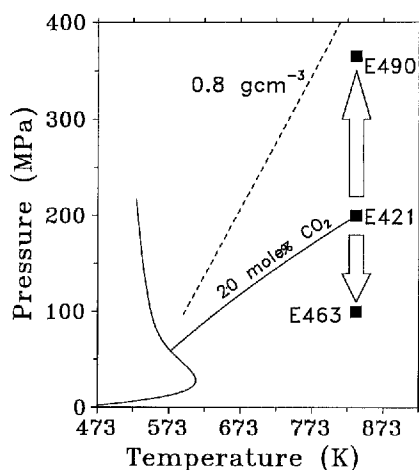


**Fig. 1.** Pressure-Temperature diagram indicating the conditions of the initial experiment E421 and re-equilibration experiments E463 and E490, black squares, which have been extensively described by Bakker and Jansen (1991). The 20 mol%  $\text{CO}_2$  isochore, nearly straight solid line (after Kerrick and Jacobs 1981) and corresponding miscibility gap, curved solid line (compilation of Töðheide and Franck 1963; Takenouchi and Kennedy 1964; Sterner and Bodnar 1991) are indicated for the initial experiment, performed at 835 K and 200 MPa. The arrows indicate isothermal compression (E490) and isothermal decompression (E463), which mimic natural evolutions of metamorphic rock. The dashed line is the isochore of  $0.8 \text{ g cm}^{-3}$  pure  $\text{H}_2\text{O}$  (Fisher 1976), which density was calculated by McLaren et al. (1983) to result from clustering of  $(4\text{H})_{\text{Si}}$  point defects in quartz.

conditions (Bakker and Jansen 1991). Re-equilibration was performed at 835 K in the presence of distilled water at either 100 MPa (E463 in Fig. 1) or 365 MPa (E490 in Fig. 1). These conditions caused either an internal overpressure or underpressure in the synthetic fluid inclusions. In both experiments, preferential  $\text{H}_2\text{O}$  leakage caused a wide range of inclusion composition and density as a result of local variation in the degree of hydrothermal recrystallization. The experimental procedure was tested with short runs (Bakker and Jansen 1991) to identify inclusion changes as a result of starting and quenching processes. No significant changes in inclusion composition and density occurred, indicating that all modification must have taken place at experimental conditions.

Samples from the experiments of Bakker and Jansen (1991) were used for microstructural investigation in the TEM. The experimentally treated Brazilian quartz crystals were then prepared by ion-bombardment from  $\pm 15 \text{ mm}$  thin sections and examined in a JEOL 200 electron microscope, operating at 200 kV. Due to the apparent hexagonal symmetry of quartz, no distinction was made between the  $a_1$ ,  $a_2$ , and  $a_3$  axes (Frondel 1962) for the identification of the orientation of the crystal-image. Consequently, no distinction was made between  $r$  and  $z$  planes.

## Microstructural observations

Several stages of the evolution of an experimentally healed crack with numerous synthetic fluid inclusions in Brazilian quartz were studied using TEM.

### Microstructural characteristics of starting material

The gem-quality Brazilian quartz appears to be optically undeformed and free of primary fluid inclusions. No crys-

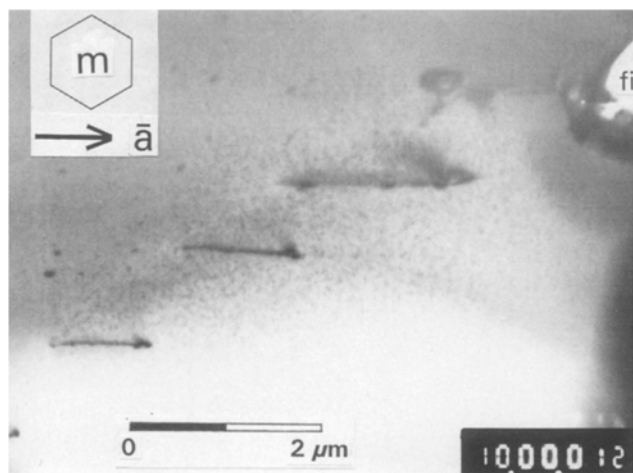


**Fig. 2.** Bright field electron micrograph (TEM) of a healed crack after the initial experiment E421. The orientation of the micrograph is indicated with a hexagon, representing the intersection of prismatic planes,  $m$ , of quartz with the photographic plane of projection. The crystallographical direction  $\bar{a}$  is expressed with the arrow. Five parallel dislocations, straight black lines, are present between fluid inclusions,  $fi$ . The black spots between the dislocations are electron beam damage centres

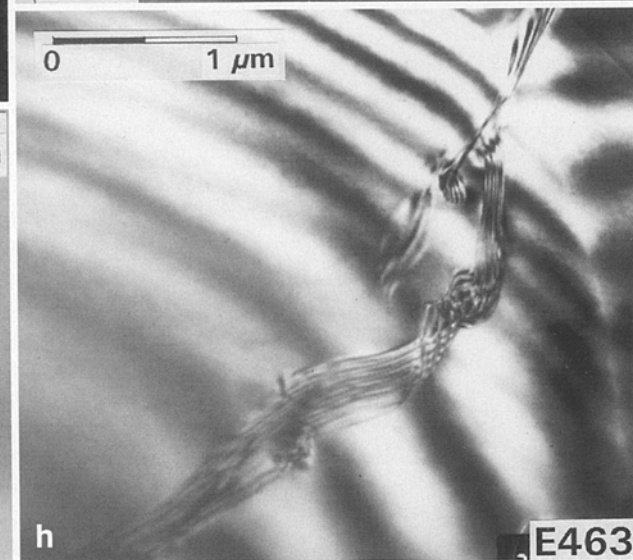
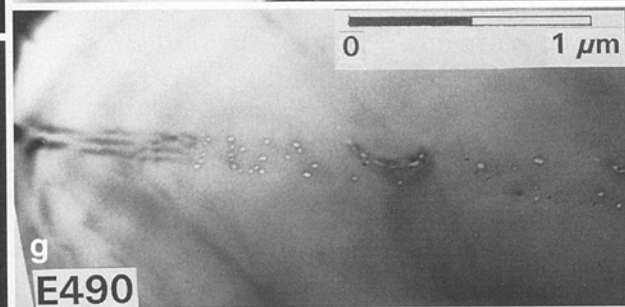
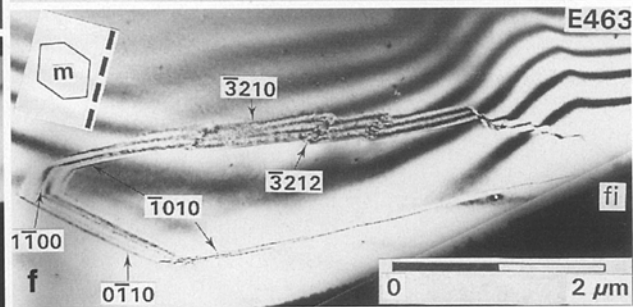
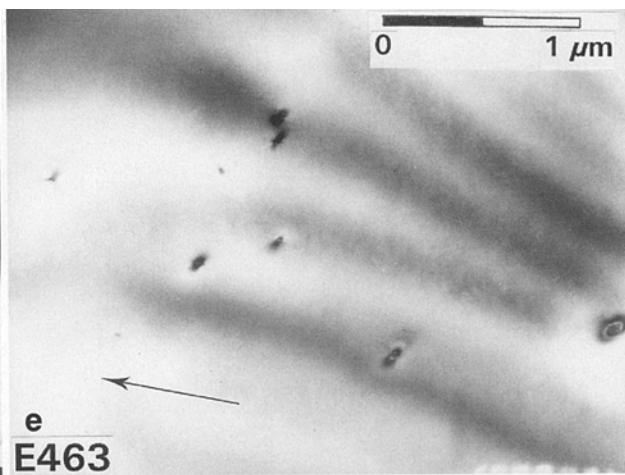
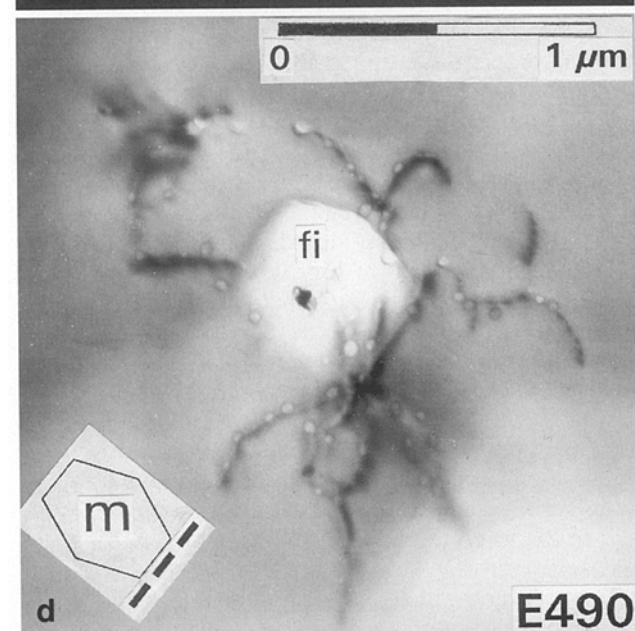
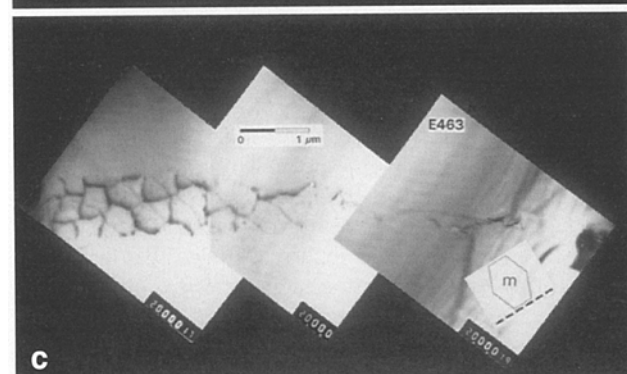
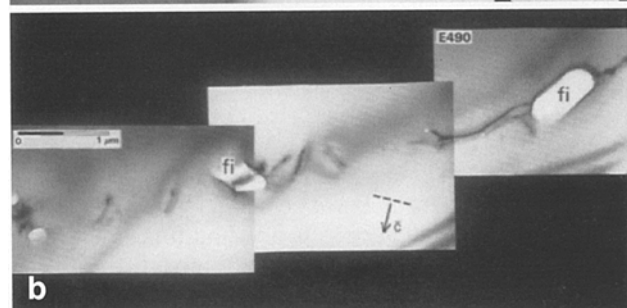
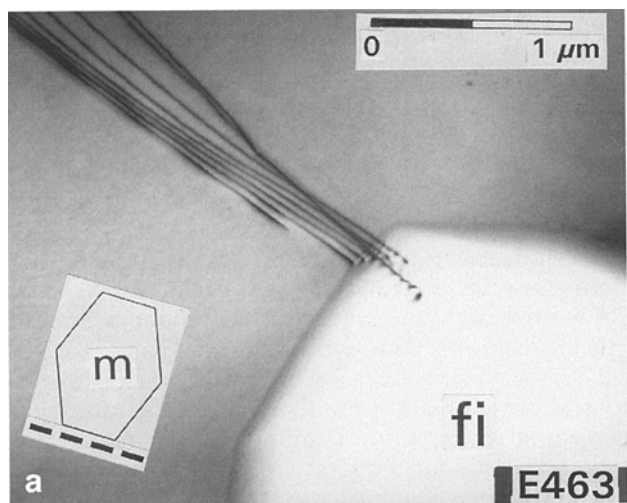
tal defects and inclusions were detected with TEM in the original starting material. The quartz seems to have a perfect crystal structure.

#### *Microstructural characteristics of healed fractures*

A quartz core with healed cracks, prepared during the initial experiment at 835 K and 200 MPa (E421 in Fig. 1) was investigated with TEM, before re-equilibration. Because primary fluid inclusions are absent, quartz between individual inclusions within a trail is identified as newly grown quartz in healed microcracks. Elongated flat synthetic fluid inclusions (Fig. 2) are recognized within healed cracks of  $\sim 1.5 \mu\text{m}$  thickness, and a maximum length/width ratio of 10:1. Newly formed fluid inclusions are often elongated in appearance with their long sides coinciding with the original crack walls, and the short sides defined by newly grown quartz in the crack. Several straight dislocation lines (Fig. 2) are observed with projected orientations parallel to a crystallographic  $\bar{a}$  direction. The apices of the dislocations mark the position of the former crack wall. The dislocation lines are oblique to the former crack wall. The Burger's vector has not been characterized. The rare and heterogeneous occurrence of dislocations justifies the assumption that the crystal defect density in healed cracks is very low. Bakker and Jansen (1991) indicate a similar occurrence of dislocations in a healed microcrack after the same initial experiment E421. In Fig. 2 several electron beam damage centres are easily recognized, which have nucleated at the crystal and grow with a noticeable speed. In general, quartz samples which have been exposed to an electron beam for more than half an hour show electron beam damage centres.

#### *Microstructural detail around re-equilibrated inclusions*

The number and variety of crystal defects in the re-equilibrated samples (E463 and E490) are much higher than the initial experiment E421. The TEM micrographs of defect structures from both re-equilibrated samples are indistinguishable and are shown in Fig. 3. The crystal defects observed seem to be restricted to the newly grown quartz within the healed cracks. The occurrence of dislocations is associated with inclusions of variable sizes. A set of seven straight subparallel dislocations are connected to an inclusion with a diameter of  $4 \mu\text{m}$  (Fig. 3A). Their projected orientations are parallel to the trace of the basal plane (0001) of quartz. The walls of the inclusion approach simple prismatic crystalline faces, which are characteristic for  $\alpha$ -quartz crystallographic orientations. A similar configuration was described by Bakker and Jansen (1990) for internally underpressurized inclusions at lower temperature (673 K). Figure 3B shows a trail of fluid inclusions with a diameter varying between 0.3 and  $0.7 \mu\text{m}$ . The rhombohedral planes of the inclusion wall are strongly developed compared to the prismatic planes. Several irregularly curved dislocations occur within the healed cracks between these inclusions. Small strain-free spheroidal bubbles of  $\sim 20 \text{ nm}$  diameter are located both at these dislocations and isolated within the trail of fluid inclusions. The small bubbles were not previously observed in either the original Brazilian natural quartz, or in the newly grown quartz in healed fractures before re-equilibration. Dislocations may be arranged in a hexagonal network (Fig. 3C) within a healed crack. The network does not exceed the position of the former crack walls, and is occasionally the boundary between the original Brazilian quartz and the newly grown quartz. Similar to Fig. 3B, many small strain-free bubbles of  $\sim 20 \text{ nm}$  diameter are visible between dislocations and several are positioned along dislocation lines. A spherical inclusion of  $0.5 \mu\text{m}$  diameter (Fig. 3D) is connected to irregularly curved dislocations with variable orientations. Each dislocation has up to twelve small strain-free bubbles of approximately 35 nm diameter. In total 62 small bubbles form a halo in a three dimensional spatial arrangement around the larger inclusions. Healed cracks are also marked by numerous features which are disk-shaped in the centre and have at both sides equal shaped strain contrast halos (Fig. 3E). They have a maximum diameter of about 100 nm. The centre lines of all disks seem to be parallel orientated. Planar defect structures, which are visible as fringe patterns in Fig. 3F, are connected to inclusions. The patterns have distinct crystallographic orientations parallel to  $\{1010\}$ ,  $\{3210\}$ , and  $\{3212\}$ . These orientations were obtained by tilting the specimen until the planar defect was parallel to the beam direction, and by using several TEM micrographs with different orientations (Appendix). The  $\{1010\}$  are arranged in a prismatic configuration. Some of these defects curve smoothly to a  $\{3210\}$  orientation, as exemplified by the edged-on defect in Fig. A1b (Appendix). The  $\{3212\}$  planes form small steps between the larger  $\{3210\}$  planes. Thickness extinction contours are discontinuous across the fringe pattern in Fig. 3F, and the ratio of spacing between the



contours on both sides is approximately 2:3. The fringe pattern seems to be symmetrical in the bright field mode of the electron microscope for several orientations of the micrographs (Fig. A1, Appendix). Previously mentioned disk-shaped features (Fig. 3E) are observed near the fringes in Fig. 3F. A wide trail of small strain-free bubbles  $\sim 20$  nm diameter, which pass into a fringe pattern are shown in Fig. 3G. An additional fringe on passing a thickness extinction contour is created by forking of the central fringe. The termination of this pattern is a series of five small bubbles, which are located on a dislocation line. The dislocation line itself is out of contrast (Fig. 3G). A fringe pattern, demonstrated in Fig. 3H, characterises a smoothly curved plane and is not related to simple crystallographic orientations. Overlapping fringes result in a mosaic pattern.

### Interpretation of microstructures

The electron beam damage centres (Fig. 2) at the surface of the specimen and the disk-shaped features in Fig. 3E and F have apparently similar occurrences. However, the disk-shaped features were present in the samples from the beginning of exposure, and did not change in shape during the exposure time. Therefore, they seem to be comparable with the features described by McLaren et al. (1983) in synthetic quartz and natural amethyst. They suggested that the features represented small lens-shaped  $H_2O$  inclusions with high densities ( $\sim 0.8 \text{ g cm}^{-3}$ ), whose strain image was inferred by Ashby and Brown (1963). The presence of similar features in Fig. 3E and F is re-

stricted to the healed cracks, and therefore they indicate the extent of the newly grown quartz. Furthermore, their presence suggests that the amount of  $H_2O$  in the healed cracks is higher than in the original Brazilian quartz. Gerretsen et al. (1989) observed similar features in epitaxial overgrowth of a single crystal. They calculated that the total amount of  $H_2O$  incorporated in the overgrown crystal is present in small fluid inclusions.

Halo textures of small bubbles around a larger fluid inclusions were suggested by Roedder (1965) to result from partial decrepitation of these primary inclusions, caused by their internal overpressure during uplift of the rock. Consequently, crack healing around these primary inclusions produces numerous smaller secondary inclusions, which occur in planes. In Fig. 3D, the small strain-free bubbles around the larger internally underpressurized synthetic fluid inclusions occur exclusively on dislocation lines with variable orientation in a three dimensional spatial arrangement, and thus are distinguishable from the secondary inclusions described by Roedder (1965). Therefore, the bubbles are proposed to develop through growth at dislocations during re-equilibration, resulting from quartz dissolution at specific spots at dislocations, transportation along dislocations, and precipitation in the larger fluid inclusion. The total volume of the small bubbles in Fig. 3D is about 10% of the volume of the central inclusion. The growth of small bubbles around internally underpressurized fluid inclusions is proposed to lead to optical visible 'implosion halos' (see Discussion), which have been recognized by Sterner and Bodnar (1989) and Bakker and Jansen (1991).

Brewster (1835) had already noted that the pressures exerted by fluid inclusions were sufficient to produce strain in crystals. Stretching of fluid inclusions was investigated by Larson et al. (1973), Bodnar and Bethke (1984), Pêcher (1984), Gratier and Jenaton (1984), but the operative deformation mechanisms were poorly understood. Carstens (1968) and Wilkins et al. (1992) noted clouds of dislocations around fluid inclusions in natural quartz, which were assumed to have formed due to stress concentration on inclusion walls. Annealing experiments at 0.1 MPa were performed by McLaren et al. (1983) and Wannamakers and Evans (1989) to investigate the hydrolytic weakening effect of quartz and the stretching mechanism of olivine, respectively. In both experiments, the pressure difference between fluid inclusions and the experimental setting was suggested to cause dislocation formation on inclusion walls. McLaren et al. (1983) found indications that dislocation loops and associated bubbles were nucleated within the strain field of small lens-shaped  $H_2O$  inclusions with high internal pressure. This assumption was confirmed by McLaren et al. (1989) for deformation experiments, and was proposed to play an important role in hydrolytic weakening of quartz. Wannamakers and Evans (1989) observed fluid density decrease and stretching of inclusions which were assumed to result from dislocation creep. They suggested that the difference between the internal pressure in fluid inclusions and the external pressure produces dislocations on the inclusion walls, which then glide or climb away from the inclusion. After thorough investigation of Fig. 1 from Wannamak-

**Fig. 3a-h.** Bright field electron micrographs (TEM) of re-equilibrated quartz cores. In **a**, **c**, **d**, and **f** the orientation of the micrograph is indicated with a hexagon, which is the intersection of prismatic planes,  $m$ , with the photographic plane of projection. The short dashed line in **a**, **b**, **c**, **d**, and **f** represents the intersection with the basal plane  $c$  of quartz. The arrow in **b** is the crystallographic direction of  $\bar{c}$ . **a** E463, A fluid inclusion,  $f_i$ , connected to seven straight dislocations. **b** E490, A trail of fluid inclusions,  $f_i$ , with several dislocations and small strain-free bubbles. Focussed on the left, some bubbles are positioned at dislocations, others are isolated between fluid inclusions and dislocations. No electron beam damage centres are observed. **c** E463, A hexagonal network of dislocations, occasionally marking the former crack walls. Several strain-free bubbles occur at dislocations and others are located between dislocations. The network passes into a trail of small bubbles. **d** E490, A synthetic fluid inclusion,  $f_i$ , connected to at least eight irregularly shaped dislocations. In total 62 small strain-free bubbles are observed only at dislocation lines. **e** E463, Small features of strain contrast, which are disk-shaped in the centre, and have equal-shaped halos on both sides. No electron beam damage centres are observed. The arrow is parallel to the centre line of all features. **f** E463, Dauphiné twins connected to a fluid inclusion,  $f_i$ , which is out of focus on the right side. Determination of the crystallographic orientation of the fringe patterns is outlined in the appendix. Several disk-shaped features are noticeable near the twins. **g** E490, Fringe pattern marking a nano crack, and passing into a trail of small strain-free bubbles, marking a healed fracture. **h** E463, Irregular fringe pattern of a nano crack, resulting in a mosaic pattern at positions of overlapping fringes

ers and Evans (1989), many small bubbles are recognized on decorated dislocations surrounding a fluid inclusion. In Fig. 3B–D, the observed dislocations and bubbles around fluid inclusions within re-equilibrated quartz are suggested to have resulted from localized deformation processes and to be similar to the microstructure described by Carstens (1968), McLaren et al. (1983), Wanamakers and Evans (1989), and Wilkins et al. (1992).

After the initial experiment E421 (Fig. 2) the straight dislocations in the healed cracks are thought to be grown-in misfit dislocations. During sample preparation, before the initial experiment, non-penetrative cracking in the crystal causes a crystallographic misfit between the crack walls. Crystal defects, like dislocations, must therefore be present within the healed cracks in order to accommodate this misfit. After re-equilibration, these straight dislocations may still be present around fluid inclusions (Fig. 3A).

Fringe patterns are indicative for the presence of planar defects, like stacking faults, twins, grain boundaries, and nanocracks. A specific type of planar defect is identified through detailed analysis of the nature of the intensity profiles of the fringe patterns, as summarized by McLaren (1991). The fringe patterns in Fig. 3F correspond to diffraction contrast intensity relations described by McLaren and Phakey (1969) which they calculated to result from Dauphiné twin boundaries. The main argument for Dauphiné twinning is the discontinuity of thickness extinction contours across the fringe pattern in specific orientations of the micrographs (Fig. 3F), with a spacing ratio on both sides of approximately 2:3. The variable orientation of the pattern, which is occasionally parallel to low-index planes, like  $\{1010\}$ ,  $\{3210\}$ , and  $\{3212\}$ , is also indicative of these twin boundaries (Fron del 1962). In general, the phase transition from hexagonal  $\beta$ -quartz to trigonal  $\alpha$ -quartz during cooling is considered to introduce Dauphiné twins in the crystal. The quartz samples in our experiments were not exposed to temperatures above the phase transition, 846 K at 0.1 MPa (Hosieni et al. 1985). Therefore, stress concentration on inclusion walls must have produced these Dauphiné twins.

McLaren et al. (1989) observed fringe patterns parallel to rhombohedral planes attached to small lens-shaped  $H_2O$  inclusions (similar to the features in Fig. 3E), which were encircled by a kind of small dislocation loop. Partial decrepitation of these inclusions was suggested to result in nanocracks, which gave rise to a fringe pattern. Fractures in quartz usually do not occur along defined crystallographic orientations, but occur in irregularly curved planes (e.g. Fig. 5 in Bakker and Jansen 1991). Therefore, the fringe pattern in Fig. 3H is proposed to represent a smoothly curved nanocrack. Fracturing is expected in this sample, for the inclusions are internally overpressurized and decrepitation is likely to occur. The nature of the planar defect in Fig. 3G could not for certain be determined from the fringe pattern, but is likely to be either a nanocrack or a stacking fault. It is assumed that this defect is replaced by numerous bubbles in a perfect crystal. This healing process must have operated discontinuously, for several trails of aligned bubbles occur parallel

to the boundary with the site where the planar defect is still present.

## Discussion

We know from microthermometry and volume estimations (Bakker and Jansen 1991) that the photographed re-equilibrated inclusions have preferentially leaked  $H_2O$  resulting in lower density and relatively  $CO_2$  enriched inclusions. A quartz core with a healed crack is schematically illustrated in Fig. 4, mimicking the setting of the experimentally healed crack after the initial experiment E421. The core is subjected to a hydrostatic pressure of pure  $H_2O$  that differs from the internal pressure in fluid inclusions. The healed crack (shaded area in Fig. 4) has several grown-in misfit dislocations and a synthetic inclusion with a  $CO_2$ - $H_2O$  gas mixture. We have used this simplified model to review processes which may occur.

### Diffusion to crystal boundary

Diffusion is a process driven by concentration gradients, which for gases can be expressed as fugacity gradients, until a homogeneous distribution is obtained. Fugacity gradients do exist between the  $H_2O$ -rich inclusions with  $X_{H_2O} \approx 0.8$  and the water outside the quartz crystal during our re-equilibration experiments E463 and E490. For  $H_2O$  and  $CO_2$  the fugacities inside the inclusions are 98.2 and 542.9 MPa (Kerrick and Jacobs 1981), respectively, during both re-equilibration experiments. Outside the

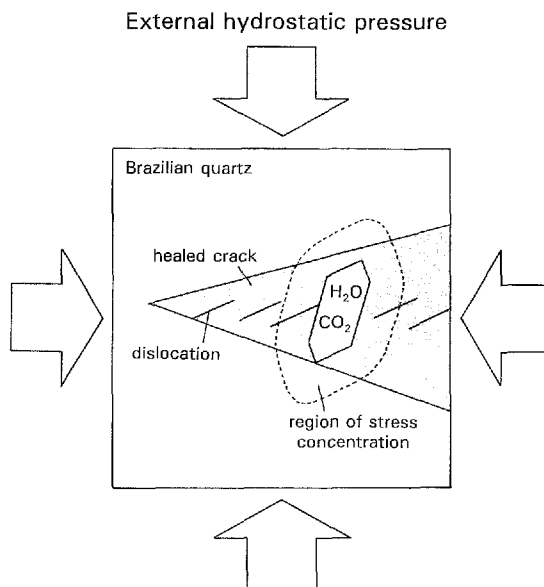


**Fig. 4.** A schematical sketch of a Brazilian quartz crystal with a healed crack, shaded area, submitted to an external hydrostatic pressure, large arrows. The healed crack contains several dislocations and a fluid inclusion with a gas mixture of  $CO_2$  and  $H_2O$ . The area within the dashed line indicates the region of stress concentration, which appears if the external pressure differs from the pressure inside the inclusions during both re-equilibration experiments E463 and E490



crystal the  $\text{H}_2\text{O}$  fugacity is 57.2 and 170.4 MPa for E463 and E490, respectively, while  $\text{CO}_2$  is absent. Therefore, if there is any communication between the inclusions and the crystal boundary, these gradients would stimulate  $\text{H}_2\text{O}$  diffusion out of internally overpressurized inclusions (E463) and into internally underpressurized inclusions (E490), while in both experiments  $\text{CO}_2$  would diffuse out of inclusions. Our observations, including preferential leakage of  $\text{H}_2\text{O}$  and nearly constant  $\text{CO}_2$  contents for both type of re-equilibration experiments (Bakker and Jansen 1991) are not in accordance with the expected effects of this gradient. Furthermore, means of communication, like penetrative microcracks or dislocations which connect inclusions to crystal boundaries appear to be absent for many inclusions that have leaked, and bulk diffusion through quartz, as previously mentioned, is not able to produce the observed amount of leakage.

The same fugacity gradient between the gas mixture inside the inclusions and the fluid outside the crystal causes a stress concentration in a rim around inclusions (Fig. 4) during both re-equilibration experiments. The crystal adjacent to the inclusions will be strained by creep mechanism, similar to the processes described by Carstens (1968), McLaren et al. (1983), and Wilkins et al. (1992) in quartz, and dislocations and planar defects are nucleated on the inclusion walls. This deformation process will be highly effective in a healed crack (shaded area in Fig. 4), where the newly grown quartz is assumed to be 'wet'. Our TEM observations (Fig. 3) indicate that the amount of crystal defects near synthetic fluid inclusions is much higher in re-equilibrated samples than in the initially healed fractures.

#### *Interaction between dislocations and $\text{H}_2\text{O}$ - $\text{CO}_2$*

The physical and chemical interaction between water and dislocations in quartz was suggested to play an important role in hydrolytic weakening (e.g. Griggs and Blacic 1965; Griggs 1974). In general, theoretical considerations on diffusion along dislocations show that the activation energy is lower (Hirth and Lothe 1968) and the diffusion coefficient is higher (Yund et al. 1981) than those for bulk-diffusion. Calculations of Heggie and Jones (1987) and Heggie (1992) indicated that, theoretically, water could both hydroxylate silicon-oxygen bonds in dislocations, and move easily as  $\text{H}_2\text{O}$  molecules along the dislocation cores without dissociation. Griggs (1974) considered enhanced solubility of water in the crystal around dislocation cores. Bakker and Jansen (1990, 1991) and Hollister (1990) adopted these concepts of the hydrolytic weakening phenomenon in quartz to model preferential  $\text{H}_2\text{O}$  leakage of fluid inclusions along dislocations. Additionally, assuming that the wetting characteristics of  $\text{H}_2\text{O}$  in microcracks (Watson and Brenan 1987) is similar to dislocation cores, water molecules could be wicked out of a homogeneous mixture of  $\text{H}_2\text{O}$  and  $\text{CO}_2$ . Therefore, we consider dislocations as small tubes, and during our experiments it is proposed that they will spontaneously attract water molecules if they are connected to  $\text{H}_2\text{O}$ -rich sources, like fluid inclusions.

A positive correlation between dislocation density and non-decrepitative  $\text{H}_2\text{O}$  leakage was inferred from deformation experiments performed by S.W.J. den Brok (personal communication 1992), who synthesized  $\text{H}_2\text{O}$ -rich inclusions in single Brazilian quartz crystals. In an attempt to homogenize the  $\text{H}_2\text{O}$  liquid and vapour phases in the inclusions during heating on a heating-freezing stage connected to an optical microscope, non-decrepitative leakage occurred before the homogenization temperature was reached. Deformation of the quartz crystal must have resulted in a very high dislocation density around inclusions, which provides many routes for  $\text{H}_2\text{O}$  leakage.

The physical and chemical interaction between  $\text{CO}_2$  and dislocations has never been a subject of investigation. Belonoshko (1989) studied the properties of a  $\text{CO}_2$ - $\text{H}_2\text{O}$  mixture in cylindrical pores of 0.8 to 2.5 nm diameter. According to his adsorption calculations, the fluid in a pore of less than 2.5 nm diameter is  $\text{H}_2\text{O}$ -richer than the bulk fluid. Therefore, dislocation cores are proposed to be rich in  $\text{H}_2\text{O}$  and block the core for  $\text{CO}_2$ , even at high temperatures and pressures. Intuitively,  $\text{CO}_2$  molecules which are about twice as large as  $\text{H}_2\text{O}$  molecules, are too large for effective  $\text{CO}_2$  pipe diffusion. The chemical interaction between quartz and  $\text{CO}_2$  is negligible.

#### *Crystal energies involving strain-free bubble nucleation on dislocations*

Saturation of all dislocations and planar defects in a rim around internally overpressurized and underpressurized synthetic fluid inclusions with water molecules can not account for the total observed amount of preferential  $\text{H}_2\text{O}$  leakage. Likewise, bulk diffusion of water-related point defects is not an effective mechanism to remove  $\text{H}_2\text{O}$  from our re-equilibrated inclusions, as previously mentioned.

Theoretical considerations of Cordier et al. (1988) indicate that water-related point defects are likely to occur in small clusters, which they reason to be energetically more favourable than randomly distributed point defects. They suggest that larger clusters may grow at the expense of smaller clusters in a quartz matrix through bulk diffusion, driven by minimalization of the total surface energy of all clusters during annealing experiments in quartz. Although the disk-shaped features observed in Fig. 3E and F may have been subjected to these processes, we will argue that water diffusion is more likely to occur along dislocations, and that strain-free bubbles develop on dislocations during our re-equilibration experiments. The occurrence of almost all strain-free bubbles on dislocation lines (Fig. 3D) is consistent with these assumptions.

A system will always tend to minimize its Gibbs free energy. A quartz crystal containing dislocations can always reach a lower energy state by reducing the total length of dislocations, which is usually referred to as a process of recovery (e.g. Hirth and Lothe 1968; Nicolas and Poirier 1976). At the surface of quartz crystals, the immediate areas around outcropping dislocations, which are elastically strained, are favourable sites for dissolu-

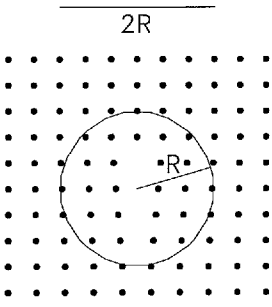


**Fig. 5.** A schematic sketch of a crystal lattice with an edge dislocation. Nucleation of a small bubble, circle, with radius,  $R$ , is replacing a dislocation with length,  $2R$ . The remaining lattice is less distorted than the elastically strained atoms within the circle

tion, resulting in the formation of etch pits (Lasaga and Blum 1986). They outlined several concepts of Gibbs free energy, contributing to the formation of etch pits at the surface, which are adopted here to establish an energy balance for bubble nucleation on dislocation lines in the crystal. This process is schematically indicated in Fig. 5, where the elastically strained atoms in the circle with radius  $R$  are assumed to dissolve and to migrate along the dislocation core, producing a small bubble.

The nucleation of a bubble with variable radius ( $dr$ ) produces a decrease in mineral volume ( $dV = -4\pi r^2 dr$ ) and an increase in surface area ( $dA = 8\pi r dr$ ). The strain energy distribution ( $u$ ) associated with a dislocation line (Eq. 1) increases the internal energy of the crystal (e.g. Hirth and Lothe 1968; Van der Hoek et al. 1982).

$$u^{\text{disl}}(r) = \frac{\mu b^2}{8\pi^2 r^2 K} \quad (\text{Eq. 1})$$

where  $\mu$  is the shear modulus,  $b$  is the Burgers vector,  $r$  is the radial distance from the dislocation, factor  $K$  is 1 for screw dislocations, and  $K$  is  $1-\nu$  for edge dislocations, where  $\nu$  is the Poisson's ratio. The elastic continuum theory breaks down within the radius of the dislocation core ( $r_0$ ), and the crystal energy which is stored in this region is undifferentiated in the factor  $\Delta E^{\text{core}}$ . Change in configuration entropy and in vibrational energy of the lattice which resulted from the presence of a dislocation are neglected (Cottrell 1953; Blum et al. 1990). Therefore, removal of the elastically strained material around dislocations will decrease the amount of crystal energy.

The total change in Gibbs free energy for the nucleation of a bubble on a dislocation line is given by Eq. 2.

$$dG = \left[ P + \frac{\Delta G^{\text{dm}}}{V_M} - u^{\text{disl}}(r) \right] dV + \gamma dA \quad (\text{Eq. 2})$$

where  $P$  is the pressure inside the bubble,  $\Delta G^{\text{dm}}$  is the change in Gibbs free energy of dissolution and migration,  $V_M$  is the molar volume of quartz, and  $\gamma$  is the surface tension. The dynamics of formation of a bubble with radius  $R$  on a dislocation line with length  $2R$  (Fig. 5) will depend on the topology of the integrated Gibbs free energy curve (Eq. 3) derived from Eqs. 1 and 2.

$$\Delta G^{\text{bubble}} = \int_0^r \left( \frac{dG}{dr} \right) dr \quad (\text{Eq. 3})$$

$$\Delta G^{\text{bubble}} = \int P dV + \frac{\Delta G^{\text{dm}}}{V_M} \frac{4}{3} \pi R^3 - \frac{\mu b^2}{2\pi K} (R - r_0) - \Delta E^{\text{core}} + \gamma 4\pi R^2$$

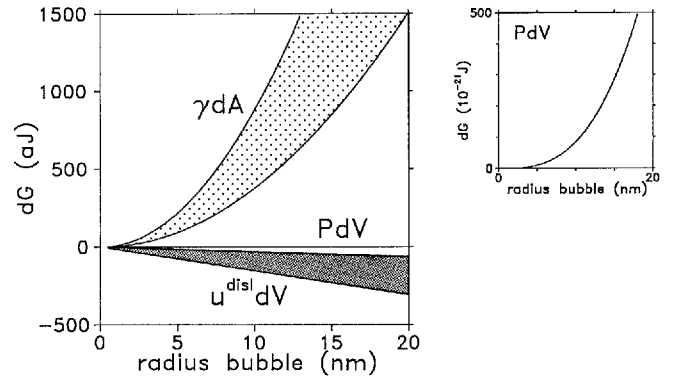


**Fig. 6.** Diagram indicating the individual contributions of dislocations, dark shaded area ( $u^{\text{disl}} dV$ ), surface tensions of small bubbles, light shaded area ( $\gamma dA$ ), and pressure in bubbles ( $PdV$ ) to the total change in Gibbs free energy (in  $\text{aJ} = 10^{-18} \text{ J}$ ) during the nucleation of a bubble on a dislocation line. On the right side, the diagram is vertically extended with a factor 1000 to indicate that the  $PdV$  term is very small ( $\sim 5 \cdot 10^{-19}$  for bubble with radius 18 nm), even for a  $\text{H}_2\text{O}$  fluid density of  $0.8 \text{ gcm}^{-3}$  inside the bubble

Lasaga and Blum (1986) reviewed selected surface tensions, shear moduli, Burgers vectors, and radii of dislocation cores in quartz, which are reasonable for a qualitative analysis of the changes in Gibbs free energy. We give a short summary of the selected values that are used for our calculations. Surface tensions ( $\gamma$ ) vary between  $0.3$  and  $0.7 \text{ Jm}^{-2}$ , which is approximately the range of estimated values between quartz and  $\text{H}_2\text{O}$  (Brace and Walsh 1962; Parks 1984; Holness et al. 1992). We have used a shear modulus ( $\mu$ ) of  $50 \text{ GPa}$ , which is regarded to be a maximum value (Heinisch et al. 1975; Heggie and Nylén 1984; Wintsch and Dunning 1985). The length of the Burgers vector ( $b$ ) varies between  $0.49$  and  $0.73 \text{ nm}$ , which is theoretically estimated with unit-cell parameters of quartz (e.g. Hosieni et al. 1985). The radius of a dislocation core ( $r_0$ ) is chosen to be equal to the length of the Burgers vector  $b$ . Most arbitrarily chosen values for  $r_0$  vary between  $b$  and  $2b$  (Franck 1951; Wintsch and Dunning 1985; Lasaga and Blum 1986; Cordier et al. 1988). Heggie and Nylén (1984) defined core energies between  $10^{-9.21}$  and  $10^{-8.17} \text{ Jm}^{-1}$  for distinct dislocations in quartz. Blum et al. (1990) neglected the core energy which was calculated to be less than  $6\%$  of the total strain energy.

The individual contributions of dislocations, surface tensions, and internal pressure to the total change in Gibbs free energy in Eq. 3 are indicated in Fig. 6. We have used a modified Redlich-Kwong equation of state for gases (DeSantis et al. 1974; Holloway 1981) to estimate the contribution of the  $PdV$  term in Eq. 3:

$$\int_0^r P dV = \int_0^r \left[ \frac{n_T R^* T}{V - n_T b^*} - \frac{n_T^2 a^*}{V(V + n_T b^*) \sqrt{T}} \right] dV \quad (\text{Eq. 4})$$

where  $R^*$  is the gas constant,  $a^*$  is the forces of attraction between molecules,  $b^*$  is the volume of individual molecules,  $V$  is the total volume of the bubble ( $4/3 \pi r^3$ ),  $T$  is the temperature, and  $n_T$  is the total amount of moles  $\text{H}_2\text{O}$  in the bubble defined by Eq. 5.

$$n_T = m \frac{4}{3} \pi r^3 \quad (\text{Eq. 5})$$



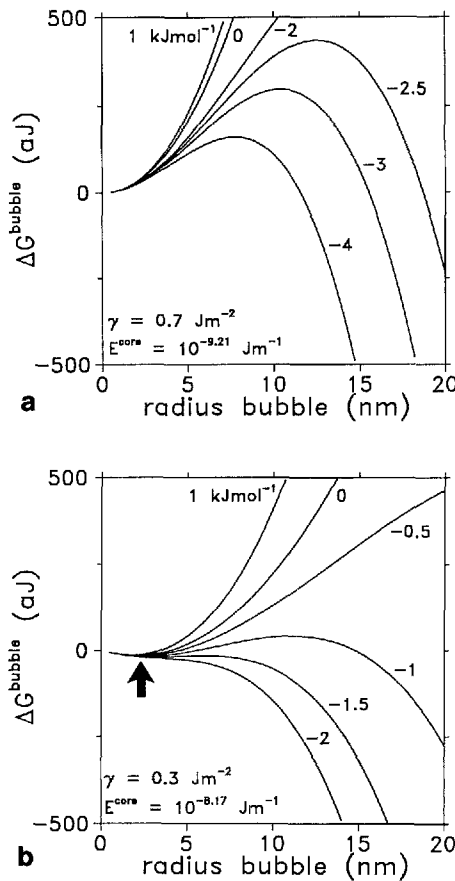


**Fig. 7.** Two diagrams of the total change in Gibbs free energy ( $\Delta G_{\text{bubble}}$ ) in aJ ( $= 10^{-18}$  J) during the nucleation and growth of a bubble with variable radius (in nm) at the expense of a dislocation line, for selected values of surface tension and dislocation core energy of  $0.7 \text{ Jm}^{-2}$  and  $10^{-9.21} \text{ Jm}^{-1}$ , respectively in (a) and  $0.3 \text{ Jm}^{-2}$  and  $10^{-8.17} \text{ Jm}^{-1}$ , respectively in (b). Each curve is calculated for a chosen value of dissolution/migration Gibbs free energy ( $\Delta G^{\text{dm}}$  indicated in  $\text{kJmol}^{-1}$ ). The existence of a minimum, arrow, for any value of  $\Delta G^{\text{dm}}$  in b allows bubbles to nucleate with a stable radius of  $\sim 2$  nm. A minimum is not observed in a, which indicates that the dislocation remains stable. For negative values of  $\Delta G^{\text{dm}}$ , small bubbles may continuously grow if an energy barrier is overcome (in a and b), which vanishes for extremely low values of  $\Delta G^{\text{dm}}$  ( $-1.5 \text{ kJmol}^{-1}$  in b).

where  $m = \rho MW^{-1}$  ( $\rho$  is the density, and  $MW$  is the molecular weight of water). Equation 5 is substituted and  $dV$  is replaced by  $4\pi r^2 dr$  in Eq. 4 to obtain a solution:

$$\int_0^r P dV = \left[ \frac{mR^*T}{1-mb^*} - \frac{m^2 a^*}{(1+mb^*)\sqrt{T}} \right] \frac{4}{3} \pi r^3 \quad (\text{Eq. 6})$$

A maximum value for Eq. 6 is obtained by using the model of McLaren et al. (1983), where clustering of  $(4\text{H})_{\text{Si}}$  defect substitutes produces small  $\text{H}_2\text{O}$  bubbles with a density of  $0.8 \text{ gcm}^{-3}$ . It is shown in Fig. 6 that the internal pressure of small bubbles accounts for a very small part of the total change in Gibbs free energy, and can be neglected. The density of small strain-free bubbles in Fig. 3B–D is probably lower than the value calculated by McLaren et al. (1983), because elastic strain induced by high pressure which resulted from this high density would have been detected easily with TEM (as in Fig. 3E,F) and is not observed around these strain-free bubbles.

The value of  $\Delta G^{\text{dm}}$  may have great impact on the free energy in Eq. 3 (Fig. 7). The exact value of  $\Delta G^{\text{dm}}$  which is dependent on dissolution and migration processes is difficult to obtain, and may change during experimentation. Therefore, the curves are calculated for variable  $\Delta G^{\text{dm}}$  values and pronounced surface tensions and dislocation core energies ( $\gamma = 0.7 \text{ Jm}^{-2}$  and  $\Delta E_{\text{core}} = 10^{-9.21} \text{ Jm}^{-1}$  in Fig. 7A, and  $\gamma = 0.3 \text{ Jm}^{-2}$  and  $\Delta E_{\text{core}} = 10^{-8.17} \text{ Jm}^{-1}$  in Fig. 7B). For  $\Delta G^{\text{dm}} = 0$ , the curve in Fig. 7B shows a minimum without an energy barrier to nucleate a bubble with a stable radius of  $\sim 2$  nm. The minimum does not exist for higher surface tensions ( $0.7 \text{ Jm}^{-2}$  in Fig. 7A) and here the dislocation will not be replaced by a bubble. Therefore, different crystallographic orientations with different surface tensions will behave differently during bubble nucleation. The question considered here is the effect of a non-zero  $\Delta G^{\text{dm}}$ . The minimum remains present in Fig. 7B for a positive  $\Delta G^{\text{dm}}$ , and a bubble with radius  $\sim 2$  nm seems to be stable. In almost all cases with a negative  $\Delta G^{\text{dm}}$ , the  $\Delta G_{\text{bubble}}$  curve exhibits a maximum, and for increasing bubble radii the curve is monotonically decreasing. For a negative  $\Delta G^{\text{dm}}$ , for example  $-1 \text{ kJmol}^{-1}$  in Fig. 7B, a bubble will be nucleated with an initial radius of  $\sim 2.5$  nm at the minimum of the  $\Delta G_{\text{bubble}}$  curve ( $\sim 17 \times 10^{-18} \text{ J}$ ). Subsequently, the bubble will continue to grow if an energy barrier of  $\sim 59 \times 10^{-18} \text{ J}$  is overcome. The energy barrier to nucleate a bubble decreases for higher negative values of  $\Delta G^{\text{dm}}$  and vanishes below  $-1.5 \text{ kJmol}^{-1}$  in Fig. 7B, but remains in Fig. 7A. The  $\Delta G^{\text{dm}}$  is comparable to the bulk free energy change of the dissolution reaction of quartz, described by Lasaga and Blum (1986). The variation in activity of silica in undersaturated solutions was calculated to result in dissolution free energies between  $-1.7$  and  $-6.7 \text{ kJ/mol}$ . It is likely that  $\Delta G^{\text{dm}}$  is variable during experimentation, for  $\Delta G^{\text{dm}}$  is expected to decrease after the wearisome initial stage of bubble nucleation on a dislocation line.

These theoretical considerations indicate that bubble nucleation on dislocations is a recovery process, and that these bubbles may grow unlimited for certain values of dislocation core energies, surface tensions, and dissolution/migration free energies.

### Solubility effects

The solubility of quartz in  $\text{H}_2\text{O}$  is sensitive to both temperature and pressure (e.g. Anderson and Burnham 1965; Walther and Orville 1983). For example, at  $835 \text{ K}$  the solubility increases from about  $0.5 \text{ wt\%}$  at  $150 \text{ MPa}$  to about  $1 \text{ wt\%}$  at  $300 \text{ MPa}$ . Migration of fluid inclusions, which is caused by solubility gradients in single fluid inclusion was described for salt (Lemlein 1952; Roedder and Belkin 1980) and ice (Hoekstra et al. 1965). The driving force is a gradient in temperature, which may be as small as  $0.0015^\circ\text{C}$  across a  $10 \mu\text{m}$  diameter inclusion. On the 'hot' side of the inclusion the host mineral continuously dissolves and on the 'cold' side it precipitates. Furthermore, solubility gradients are generated by pressure differences in single crystals, and by heterogeneous dislocation distribution on inclusion walls (Roedder 1984).

For internally underpressurized inclusions (E490 in Fig. 1), the silica gradient which is caused by the pressure differences inside the crystal between fluid inclusions and the external pressure medium could provide continuously a driving force for  $\text{SiO}_2$  migration along dislocations from the smaller bubbles to the larger cavities, assuming that this pressure difference is maintained and is smoothly varying in the crystal. The small bubbles on dislocations around the large synthetic inclusion in Fig. 3D are proposed to be a preliminary stage in the development of optically visible implosion halos (Sterner and Bodnar 1989; Bakker and Jansen 1991) which did not result from partial decrepitation. These implosion halos will not develop around internally overpressurized inclusions (E463 in Fig. 1) for the pressure gradient between the external medium and the inclusion results in a reversed solubility gradient, causing the bubbles to shrink or remain a very small size.

### Naxos (Greece), a case study

The experimentally leaking fluid inclusions are in principle proposed to be an analogy to natural inclusion behaviour in complex metamorphic rocks, despite the relatively rapidly healing and quenching procedures during experimentation. This is consistent with theoretical considerations of Hollister (1988), who proposed selective leakage of  $\text{H}_2\text{O}$  from natural  $\text{H}_2\text{O}$ - $\text{CO}_2$ -rich fluid inclusions in metamorphic rock to explain the abundance of nearly pure  $\text{CO}_2$  inclusions in migmatites which were thermodynamically calculated to contain  $\text{H}_2\text{O}$ -rich fluids. Therefore, we have carefully compared microstructures around natural fluid inclusions in quartz lenses from Naxos (Greece) with the experimentally obtained results.

The metamorphism and deformation of natural rock from Naxos (Greece) were extensively investigated by Jansen and Schuiling (1976), Andriessen et al. (1979), Kreulen (1980), Buick and Holland (1989, 1991), and Urai et al. (1990). An early metamorphic event, M1 (Fig. 8) was characterized by glaucophane-bearing as-

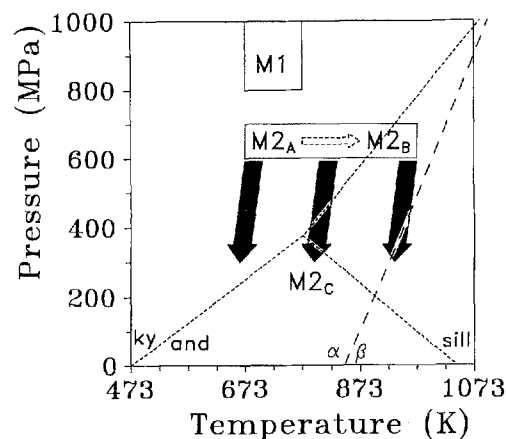
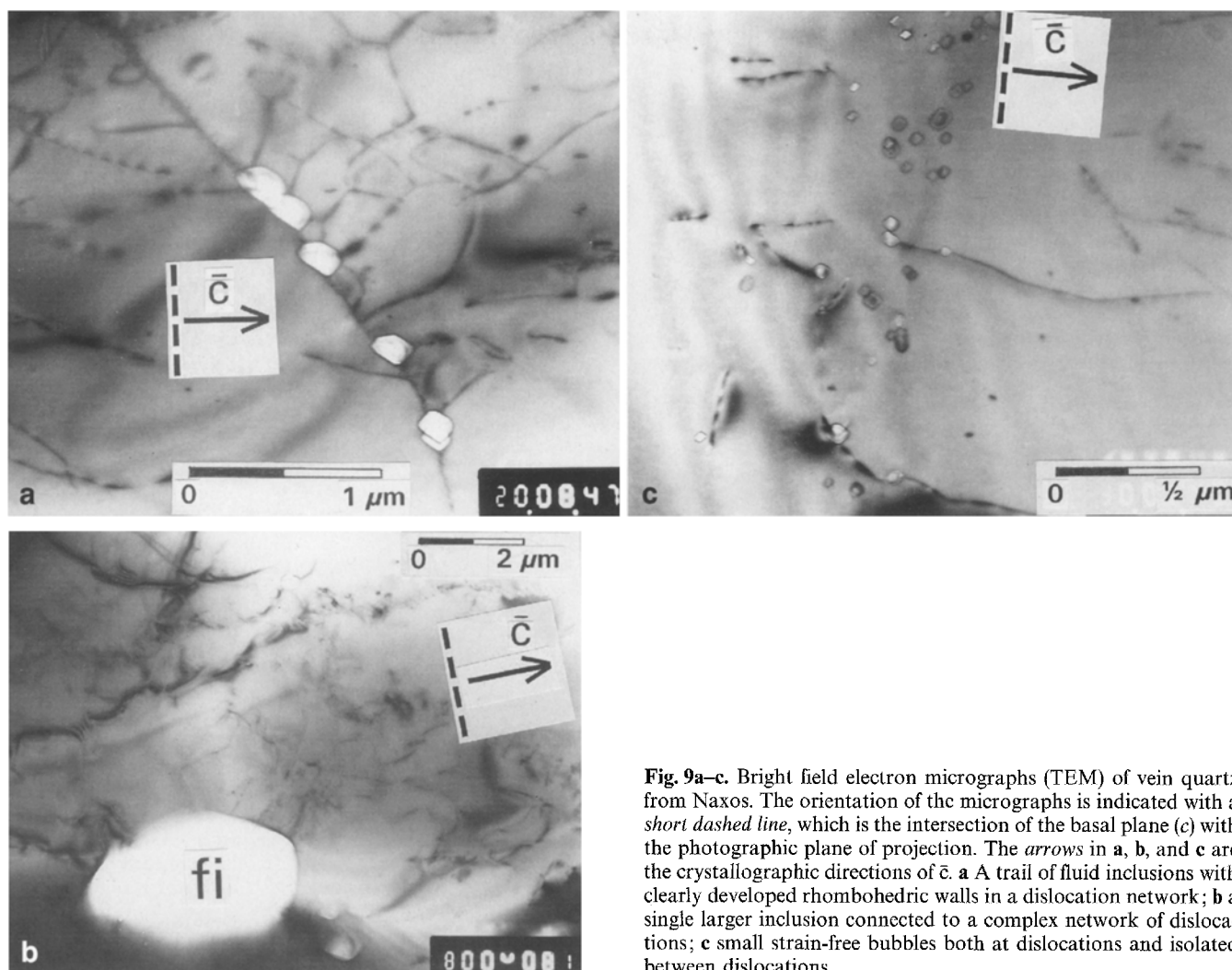


Fig. 8. Pressure-temperature diagram. Three main metamorphic events are M1, blueschist facies;  $M2_A$ , regional greenschist facies which locally reached to  $M2_B$  upper amphibolite facies; and  $M2_C$ , the metamorphism after uplift of the complex during extensional thinning of the crust (indicated with 3 solid arrows). The short dashed lines indicate the triple point of the  $\text{Al}_2\text{SiO}_5$  polymorphs (Holdaway 1971), and the large dashed line indicates the transition of  $\alpha$ -quartz to  $\beta$ -quartz (Hosieni et al. 1985).

semblages. The main metamorphic phase,  $M2_A$  and  $M2_B$  (Fig. 8) affecting Naxos formed a Barrovian facies series. The solid arrows in Fig. 8 represent pressure decrease, caused by crustal extension towards  $M2_C$ , which promoted regional exhumation of the metamorphic complex (Buick 1991). Kreulen (1980) described an abundance of peak metamorphic  $M2_B$   $\text{CO}_2$ -rich inclusions in unselective quartz lenses throughout the metamorphic complex, irrespectively of lithology, metamorphic grade, or event. A brine, which was described in several inclusions, was present at a very late stage, after  $M2_C$ , and could not have effected immiscibility properties of the fluid at peak metamorphic conditions. Many fluid densities of  $\text{CO}_2$ -rich inclusions are too low with respect to peak metamorphic  $M2_B$  conditions, and they resemble typical values for the  $M2_C$  re-equilibration. Mineral assemblages which were stable at  $M2_B$  conditions buffered volatile species to high  $X_{\text{H}_2\text{O}}$  values in epidote/zoisite bearing schists, in amphibolites, and in vesuvianite-bearing calc-silicates (Jansen and Schuiling 1976; Buick and Holland 1991). Locally, high  $X_{\text{CO}_2}$  values were determined in siliceous dolomites (Jansen et al. 1978; Buick and Holland 1991). Although, the observed mole fraction of  $\text{CO}_2$  in inclusions was not related to lithology, the carbon-isotope ( $\delta^{13}\text{C}$ ) data on experimentally decrepitated fluid inclusions in quartz lenses (Rye et al. 1976; Kreulen 1980) seemed to be characteristic in siliceous dolomites and in graphite-bearing quartzites. Therefore, compositional modification by selective leakage of  $\text{H}_2\text{O}$  must have occurred, leaving behind a  $\text{CO}_2$  enriched inclusion with lower density. Deformation-induced recrystallisation around inclusions, like decrepitation and stretching, may have affected the density, but is unlikely to affect the composition of inclusions.

### Vein quartz from Naxos

Natural quartz lenses were collected by F. Postma in Naxos. The samples were cut into 2 mm thick slices, and further thinned to 30  $\mu\text{m}$  by polishing, for characterization of the fluid inclusions composition and density. The natural vein quartz samples from Naxos are polycrystalline, and display many deformation features, which are visible with an optical microscope. Electron micrographs of quartz adjacent to natural inclusions reveal a high defect density (Fig. 9), for example at sub-grain boundaries. The inclusions are often connected to dislocation networks. In one single sample several types of fluid inclusions could be distinguished in natural quartz. Small negative  $\beta$ -quartz shaped inclusions with 0.4  $\mu\text{m}$  diameter (Fig. 9A) are arranged in a trail, and are mutually connected with dislocations in a network. The inclusion walls have a well developed negative  $\beta$ -quartz morphology. The shape of the inclusions indicates that they were formed or recrystallized at temperatures above the transition temperature of  $\alpha$ -quartz, which only occurred during the  $M2_C$  re-equilibration (Fig. 8). Large negative  $\alpha$ -quartz fluid inclusions with 4  $\mu\text{m}$  diameter (Fig. 9B) are connected to complex dislocation networks. Dislocations occur as straight and curved lines, some are parallel to c direction. Several triple junctions are present. In Fig. 9C, several small strain-free bubbles with 30 nm diameter occur at dislocation lines and isolated between dislocations. They have also well developed negative  $\beta$ -quartz morphologies. The dislocation density in these natural samples (Fig. 9) is much higher than the density in the experimentally healed cracks in Brazilian quartz (Fig. 3). Routes for preferential  $\text{H}_2\text{O}$  leakage in deformed natural vein quartz are very abundant compared to experimentally treated Brazilian quartz. The appearance of small



**Fig. 9a–c.** Bright field electron micrographs (TEM) of vein quartz from Naxos. The orientation of the micrographs is indicated with a *short dashed line*, which is the intersection of the basal plane ( $c$ ) with the photographic plane of projection. The *arrows* in **a**, **b**, and **c** are the crystallographic directions of  $\bar{c}$ . **a** A trail of fluid inclusions with clearly developed rhombohedral walls in a dislocation network; **b** a single larger inclusion connected to a complex network of dislocations; **c** small strain-free bubbles both at dislocations and isolated between dislocations

strain-free bubbles on dislocation lines in natural samples (Fig. 9C) is similar to the bubbles observed in Fig. 3B–D, indicating that similar recovery processes may have operated.

## Conclusions

The experimentally re-equilibrated  $\text{H}_2\text{O}$ - $\text{CO}_2$ -rich inclusions have preferentially leaked  $\text{H}_2\text{O}$ , resulting in relatively  $\text{CO}_2$ -enriched inclusions (Bakker and Jansen 1991). The process of non-decrepitative preferential  $\text{H}_2\text{O}$  leakage is caused by a differentiation of the fluid at a molecular scale at supercritical conditions.

Apparently, water moves up against the fugacity gradient between inclusions and the fluid at the grain boundary during experiment E490. However, this gradient is assumed not to be effective due to the lack of communication (penetrative fractures or dislocations) between inclusions and grain boundary.

The amount and variety of crystal defects around fluid inclusions which experienced internal overpressures and underpressures, is much higher compared to the initial

synthesized inclusions during crack healing. The observed defect microstructures appear to exist wholly within the new quartz in healed fractures. Pressure differences between inclusions and experimental settings result in localized plastic deformation around inclusions, nucleating many dislocations and twin boundaries on inclusion walls. The defect microstructures provide many routes for material diffusion, and preferential  $\text{H}_2\text{O}$  leakage must have occurred by selective diffusion along dislocations and twin boundaries. Theoretical considerations about  $\text{H}_2\text{O}$  and  $\text{CO}_2$  adsorption on quartz surfaces indicate that at high supercritical  $P$ - $T$  conditions  $\text{CO}_2$  is restrained from entering defect microstructures.

The transport capacity of this leakage mechanism is enhanced by the nucleation of small bubbles on defect structures. The formation of small strain-free bubbles on dislocations is proposed to reduce the internal energy of a strained crystal. This recovery process is controlled by dislocation self-energy, surface free energy of small bubbles, and dissolution/migration free energy along dislocations ( $\Delta G^{\text{dm}}$ ). For a selected surface tension of  $0.3 \text{ Jm}^{-2}$  and dislocation core energy of  $10^{-8.17} \text{ Jm}^{-1}$ , a bubble with stable radius of  $\sim 2 \text{ nm}$  will nucleate on a dislocation line

independently of  $\Delta G^{\text{dm}}$ . An activation barrier for continuous bubble growth is introduced for a negative  $\Delta G^{\text{dm}}$ , and vanishes for decreasing values of  $\Delta G^{\text{dm}}$ .

Additionally, solubility gradients of quartz in  $\text{H}_2\text{O}$  in single crystals with internally underpressurized inclusions may enhance the growth of small strain-free bubbles to optically visible implosion halos in a three-dimensional spatial arrangement at the expense of larger synthetic fluid inclusions.

Comparable processes of  $\text{H}_2\text{O}$  migration along defect microstructures and recovery processes are suggested to

be operative in natural samples. The high dislocation density and amount of small strain-free bubbles observed in quartz lenses around inclusions from Naxos (Greece) are very similar to that observed in experimentally re-equilibrated synthetic inclusions, and provide many routes for non-decrepitative preferential  $\text{H}_2\text{O}$  leakage.

**Acknowledgements.** We greatly appreciate useful reviews of the manuscript by Tom Andersen, M.R. Drury, Robert McDonnell, Pauline Mollema and Michael Sterner. This study was supported by a grant from NWO/AWON, project no. 751.353.020.

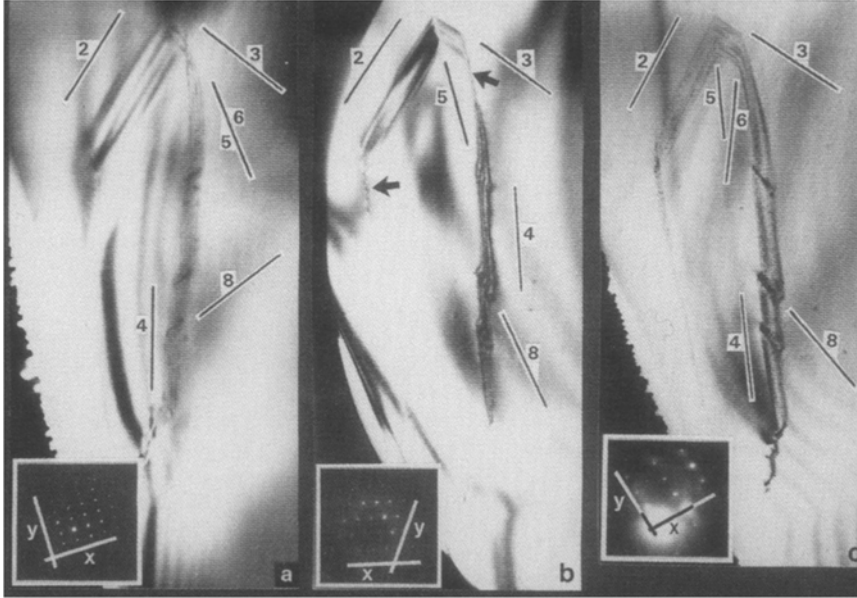


**Fig. A1a-c.** Bright field TEM micrographs of the planar defects in Fig. 3F taken at three different orientations. The corresponding diffraction spots are indexed as  $x$  and  $y$ ,  $\{11\bar{2}0\}$  and  $\{0001\}$  in (a)  $\{10\bar{1}0\}$  and  $\{1\bar{1}01\}$  in (b),  $\{20\bar{2}1\}$  and  $\{01\bar{1}1\}$  in (c) respectively. The orientation of several projected lines, which are used to measure the orientation of the planar defects, are accented with *short solid lines* (2, 3, 4, 5, 6, and 8) in each micrograph. The planar defects indicated with *arrows* in **b** are edge-on

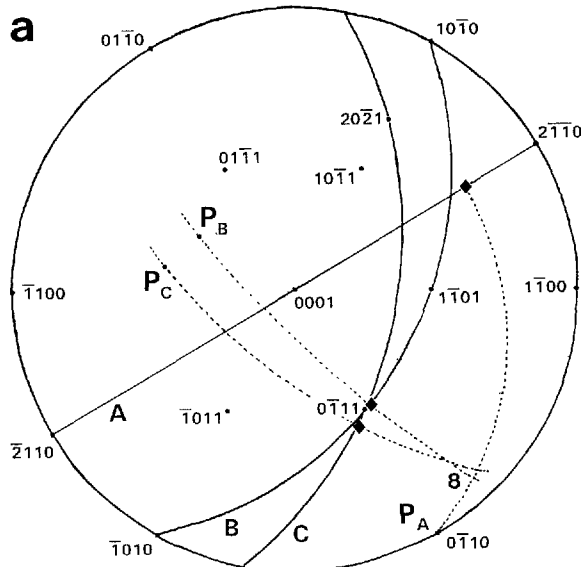
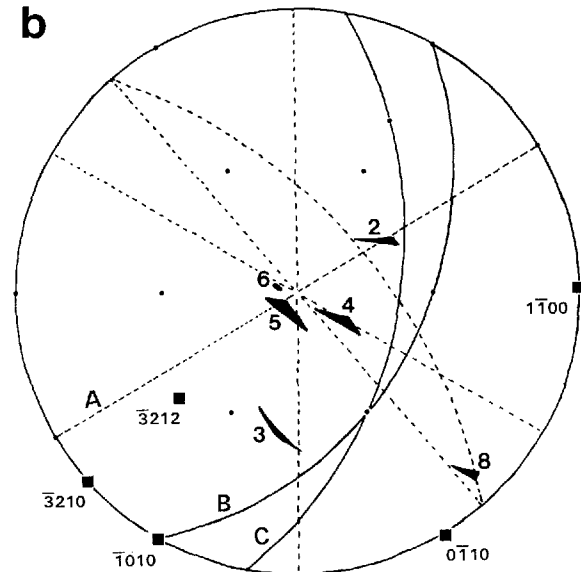


**Fig. A2a,b.** Stereographic projections in Wulff nets of crystallographic characteristics identified in the TEM micrographs of Fig. A1. **a** Basal, prismatic, and rhombohedral planes are identified with Miller-Bravais indices,  $\{0001\}$ ,  $\{10\bar{1}0\}$  and  $\{10\bar{1}1\}$ , respectively. The diffraction patterns of Fig. A1 are shown as great-circles (*solid lines* A, B, and C), corresponding to Fig. A1a,b, and c, respectively. The poles of these planes are indicated with  $P_A$ ,  $P_B$ , and  $P_C$ . The *diamonds* are projected lines of 8 from Fig. A1 in each diffrac-



tion pattern. The *dashed lines* are great-circles through the projected lines and  $P_A$ ,  $P_B$ , or  $P_C$ .

**b** The real orientation of the *lines* 2, 3, 4, 5, 6, and 8 are shown as *black smudges* which indicate the error in measurement. The *dashed great-circles* are the planes defined by these lines and seem to be crystallographically controlled. The reciprocal lattice vectors (pole) of these great-circles are indexed,  $(10\bar{1}0)$ ,  $(01\bar{1}0)$ ,  $(1\bar{1}00)$ ,  $(3\bar{2}10)$ , and  $(3\bar{2}12)$ , and indicated with *squares*

## Appendix

### Orientation of planar defects

Two methods were used to determine crystallographic orientations of planar defects in Fig. 3F:

1. The specimen was tilted in the microscope until the planar defect was parallel to the incident beam direction. The crystallographic indices of the edged-on planar defects in Fig. A1b (arrows) were identified as  $\{10\bar{1}0\}$ .
2. The specimen could not be tilted parallel to the beam for other planar defects. Therefore, determination of these planar defects is based on the principle that a plane is defined by two non-parallel lines. The lines are defined by the intersection of two planar features (e.g. lines 5, 6, and 8 in Fig. A1) or by traces of the defects in the specimen foil (e.g. lines 2, 3, and 4 in Fig. A1). Each of these lines is a projection on a TEM micrograph, therefore, several micrographs with different diffraction patterns are required to obtain the real orientation of each line. The angle between the projected line (e.g. the diamonds in Fig. A2a for line 8) and the known orientation of the diffraction pattern was measured and plotted into a Wulff net. The great-circle is determined through the projected line and the incident beam direction (e.g.  $P_A$  in Fig. A2a), which is perpendicular to the diffraction pattern. This procedure is repeated for the identical planar defect on micrographs with different orientations (Fig. A2a). Intersection of the obtained great-circles gives the required orientation of the line. The results of the measurements are shown in Fig. A2b. All planar defects were constructed from two or three lines which define a plane. The planar defects could be fitted to distinct crystallographic orientations,  $\{10\bar{1}0\}$ ,  $\{3\bar{2}10\}$ , and  $\{3\bar{2}12\}$  in Fig. A2b.

## References

- Aines RD, Kirby SH, Rossman GR (1984) Hydrogen specification in synthetic quartz. *Phys Chem Miner* 11:204–212
- Anderson GM, Burnham CW (1965) The solubility of quartz in supercritical water. *Am J Sci* 263:494–511
- Andriessen PAM, Boelrijk NAIM, Herbede EH, Priem HNA, Verdurmen EAT, Verschuren RH (1979) Dating events of metamorphism and granitic magmatism in the Alpine Orogen at Naxos (Cyclades, Greece). *Contrib Mineral Petrol* 69:215–225
- Ashby MF, Brown LM (1963) Diffraction contrast from spherical symmetrical coherency strains. *Philos Mag* 8:1083–1103
- Bakker RJ, Jansen JBH (1990) Preferential water leakage from fluid inclusions by means of mobile dislocations. *Nature* 345:58–60
- Bakker RJ, Jansen JBH (1991) Experimental post-entrapment water loss from synthetic  $\text{CO}_2$ - $\text{H}_2\text{O}$  inclusions in natural quartz. *Geochim Cosmochim Acta* 55:2215–2230
- Belonoshko AB (1989) The thermodynamics of the aqueous carbon dioxide fluid in pores. *Geochim Cosmochim Acta* 53:2581–2590
- Blum AE, Yund RA, Lasaga AC (1990) The effect of dislocation density on the dissolution rate of quartz. *Geochim Cosmochim Acta* 54:283–297
- Bodnar RJ, Bethke PM (1984) Systematics of stretching of fluid inclusions. I. Fluorite and sphalerite at 1 atmosphere confining pressure. *Econ Geol* 79:141–161
- Brace WF, Walsh JB (1962) Some direct measurements of surface energy of quartz and orthoclase. *Am Mineral* 47:1111–1122
- Brewster D (1835) Observations relative to the structure and origin of the diamond. *Trans Geol Soc London* 3:455–459
- Buick IS (1991) The late Alpine evolution of an extensional shear zone, Naxos, Greece. *J Geol Soc London* 148:93–103
- Buick IS, Holland TJB (1989) The  $P$ - $T$ - $t$  path associated with crustal extension, Naxos, Cyclades, Greece. In: Daly JS, Cliff RA, Yardley BWD (eds) Evolution of metamorphic belts. *Geol Soc London Spec Publ* 43, pp 365–369
- Buick IS, Holland TJB (1991) The nature and distribution of fluids during amphibolite facies metamorphism, Naxos (Greece). *J Metamorphic Geol* 9:301–314
- Carstens H (1968) The lineage structure of quartz crystals. *Contrib Mineral Petrol* 18:295–304
- Cordier P, Doukhan JC (1989) Water solubility in quartz and its influence on ductility. *Eur J Mineral* 1:221–237
- Cordier P, Boulogne B, Doukhan JC (1988) Water precipitation and diffusion in wet quartz and wet berlinite  $\text{AlPO}_4$ . *Bull Mineral* 111:113–137
- Cottrell AH (1953) Dislocations and plastic flow in crystals. Oxford Univ Press, Oxford
- DeSantis R, Breedveld GJF, Prausnitz JM (1974) Thermodynamic properties of aqueous gas mixtures at advanced pressure. *Ind Eng Chem Process Des Dev* 13:374–377
- Doukhan JC, Paterson MS (1986) Solubility of water in quartz – a revision. *Bull Mineral* 109:193–198
- Doukhan JC, Trepied L (1985) Plastic deformation of single quartz crystals. *Bull Mineral* 108:97–123
- Ferguson HG (1914) Lode deposits of the Alleghany district, California. *US Geol Surv Bull* 580-I: 161
- Fisher JR (1976) The volumetric properties of  $\text{H}_2\text{O}$  – a graphical portrayal. *J Res US Geol Surv* 4:189–193
- FitzGerald JD, Boland JN, McLaren AC (1991) Microstructures in water-weakened single crystals of quartz. *J Geophys Res* 96:2139–2155
- Frank FC (1951) Capillary equilibria of dislocated crystals. *Acta Crystallogr* 4:497–501
- Fronzel C (1962) The system of mineralogy of James Dwight Dana and Edward Salisbury Dana, Yale University 1837–1892. Silica minerals, vol 3. Wiley, New York
- Gerretsen J, Paterson MS, McLaren AC (1989) The uptake and solubility of water in quartz at elevated pressure and temperature. *Phys Chem Miner* 16:334–342
- Gratier JP, Jenaton L (1984) Deformation by solution-deposition, and re-equilibration of crystals depending on temperature, internal pressure, and stress. *J Struct Geol* 6:189–200
- Griggs DT (1974) A model of hydrolytic weakening in quartz. *J Geophys Res* 79:1653–1661
- Griggs DT, Blacic JD (1965) Quartz: anomalous weakness in synthetic crystals. *Science* 147:292–295
- Heggie M (1992) A molecular water pump in quartz dislocations. *Nature* 355:337–339
- Heggie M, Jones R (1987) Density functional analysis of the hydrolysis of Si-O bonds in disiloxane: application to hydrolytic weakening in quartz. *Philos Mag Lett* 55:47–51
- Heggie M, Nylén M (1984) Dislocation core structures in  $\alpha$ -quartz from a valence force potential. *Philos Mag B* 50:543–555
- Heinisch HL, Sines G Jr, Goodman JW, Kirby SH (1975) Elastic stresses and self-energies of dislocations of arbitrary orientation in anisotropic media: olivine, orthopyroxene, calcite, and quartz. *J Geophys Res* 80:1885–1896
- Hirth JP, Lothe J (1968) Theory of dislocation. McGraw-Hill, New York
- Hoekstra P, Osterkamp TE, Weeks WF (1965) The migration of liquid inclusions in single ice crystals. *J Geophys Res* 70:5053–5041
- Holdaway HJ (1971) Stability of andalusite and the aluminum silicate phase diagram. *Am J Sci* 271:97–131
- Hollister LS (1988) On the origin of  $\text{CO}_2$ -rich fluid inclusions in migmatites. *J Metamorphic Geol* 6:467–474
- Hollister LS (1990) Enrichment of  $\text{CO}_2$  in fluid inclusions in quartz by removal of  $\text{H}_2\text{O}$  during crystal-plastic deformation. *J Struct Geol* 12:895–901
- Holloway JR (1981) Compositions and volumes of supercritical fluids in the Earth's crust. In: Hollister LS, Crawford ML (eds) Short course in fluid inclusions: applications to petrology, pp 13–38
- Holness MB, Fein J, Graham CM (1992) The effect of pressure on solid-dihedral angles in the system  $\text{H}_2\text{O}$ - $\text{CO}_2$ - $\text{NaCl}$ -Quartz (ab-

- stract). Terra Abstr, IV<sup>th</sup> Int Symp Exp Mineral Petrol Geochem 4:21
- Hosieni KR, Howald RA, Scanlon MW (1985) Thermodynamics of the lambda transition and the equation of state of quartz. *Am Mineral* 70:782–793
- Jansen JBH, Schuiling RD (1976) Metamorphism on Naxos, petrology and thermal gradients. *Am J Sci* 276:1225–1253
- Jansen JBH, Van der Kraats AH, Van der Rijst H, Schuiling RD (1978) Metamorphism of siliceous dolomites at Naxos, Greece. *Contrib Mineral Petrol* 67:279–288
- Kerrick DM, Jacobs GK (1981) A modified Redlich-Kwong equation for H<sub>2</sub>O, CO<sub>2</sub>, and H<sub>2</sub>O-CO<sub>2</sub> mixtures at elevated pressures and temperatures. *Am J Sci* 281:735–767
- Kreulen R (1980) CO<sub>2</sub>-rich fluids during regional metamorphism on Naxos (Greece): carbon isotopes and fluid inclusions. *Am J Sci* 280:745–771
- Kronenberg AK, Kirby SH, Aines RD, Rossman GR (1986) Solubility and diffusional uptake of hydrogen in quartz at high water pressures: implications for hydrolytic weakening. *J Geophys Res* 91:12723–12744
- Larson LT, Miller JD, Nadeau JE, Roedder E (1973) Two sources of error in low temperature inclusion homogenization determination, and corrections on published temperatures for the East Tennessee and Laisvall deposits. *Econ Geol* 68:113–116
- Lasaga AC, Blum AE (1986) Surface chemistry, etch pits and mineral-water reactions. *Geochim Cosmochim Acta* 50:2363–2379
- Lemlein GG (1952) Migration of liquid fluid inclusions in a crystal towards a source of heat. *Dokl Akad Nauk SSSR* 85:325–328
- McLaren AC (1991) Transmission electron microscopy of minerals and rocks. (Cambridge topics in mineral physics and chemistry 2) Cambridge Univ Press, Cambridge
- McLaren AC, Phakey PP (1965) A transmission electron microscope study of amethyst and citrine. *Aust J Phys* 18:135–141
- McLaren AC, Phakey PP (1969) Diffraction contrast from Dauphiné twin boundaries in quartz. *Phys Status Solidi* 31:723–737
- McLaren AC, Cook RF, Hyde ST, Tobin RC (1983) The mechanism of the formation and growth of water bubbles and associated dislocation loops in synthetic quartz. *Phys Chem Miner* 9:79–94
- McLaren AC, FitzGerald JD, Gerretsen J (1989) Dislocation nucleation and multiplication in synthetic quartz: relevance to water weakening. *Phys Chem Miner* 15:465–482
- Nicolas A, Poirier JP (1976) Crystalline plasticity and solid state flow in metamorphic rocks. Wiley Interscience, London
- Parks GA (1984) Surface and interfacial free energies of quartz. *J Geophys Res* 89:3997–4008
- Paterson MS (1986) The thermodynamics of water in quartz. *Phys Chem Miner* 13:245–255
- Pêcher A (1984) Chronologie et ré-équilibrage des inclusions fluides: quelques limites à leur utilisation en microthermométrie. In: Lagache M (ed) *Thermométrie et barométrie géologiques*. Soc Fr Mineral Cristallogr 2:463–485
- Roedder E (1965) Liquid CO<sub>2</sub> inclusions in olivine-bearing nodules and phenocrysts from basalts. *Am Mineral* 50:1746–1782
- Roedder E (1984) Fluid inclusions. (Reviews in Mineralogy 12) Geol Soc Am, Washington, DC
- Roedder E, Belkin HE (1980) Thermal gradient migration of fluid inclusions in single crystals of salt from waste isolation pilot plant site (WIPP). *Sci Basis Nucl Waste Manage* 2:453–464
- Rovetta MR, Holloway JR, Blacic JD (1986) Solubility of hydroxyl in natural quartz annealed in water at 900°C and 1.5 GPa. *Geophys Res Lett* 13:145–148
- Rye RO, Schuiling RD, Rye DM, Jansen JBH (1976) Carbon, hydrogen, and oxygen isotope studies of the regional metamorphic complex at Naxos, Greece. *Geochim Cosmochim Acta* 40:1031–1049
- Sterner SM, Bodnar RJ (1984) Synthetic fluid inclusions in natural quartz. I. Compositional types synthesized and applications to experimental geochemistry. *Geochim Cosmochim Acta* 48:2659–2668
- Sterner SM, Bodnar RJ (1989) Synthetic fluid inclusions. VII. Re-equilibration of fluid inclusions in quartz during laboratory-simulated metamorphic burial and uplift. *J Metamorphic Geol* 7:243–260
- Sterner SM, Bodnar RJ (1991) Synthetic fluid inclusions. X. Determination of *P-V-T-X* properties in the CO<sub>2</sub>-H<sub>2</sub>O system to 6 kbar and 700°C. *Am J Sci* 291:1–54
- Takenouchi S, Kennedy GC (1964) The binary system H<sub>2</sub>O-CO<sub>2</sub> at high temperatures and pressures. *Am J Sci* 262:1055–1074
- Tödeheide K, Franck EU (1963) Das Zweiphasengebiet und die kritische Kurve im System Kohlendioxid-Wasser bis zu Drucken von 3500 bar. *Z Phys Chem Neue Folge* 37:387–401
- Urai JL, Schuiling RD, Jansen JBH (1990) Alpine deformation on Naxos (Greece). In: Knipe RJ, Rutter EH (eds) *Deformation mechanisms, rheology and tectonics*. Geol Soc Spec Publ 54, pp 509–522
- Van der Hoek B, Van der Eerden JP, Bennema P (1982) Thermodynamic stability conditions for the occurrence of hollow cores caused by stress of line and planar defects. *J Cryst Growth* 56:621–632
- Walther JV, Orville PM (1983) The extraction-quench technique for determination of the thermodynamic properties of solute complexes: application to quartz solubility in fluid mixtures. *Am Mineral* 68:731–741
- Wanamakers BJ, Evans B (1989) Mechanical re-equilibration of fluid inclusions in San Carlos olivine by power-law creep. *Contrib Mineral Petrol* 102:102–111
- Watson EB, Brenan JM (1987) Fluids in the lithosphere. 1. Experimentally determined wetting characteristics of CO<sub>2</sub>-H<sub>2</sub>O fluids and their application for fluid transport, host-rock physical properties, and fluid inclusion formation. *Earth Planet Sci Lett* 85:497–515
- Wilkins RWT, Hladky G, Gratier JP, Jenatton L (1992) Some relationships between cracks and fluid inclusions (abstract). PACROFI IV, UC Riverside, 89
- Wintsch RP, Duning J (1985) The effect of dislocation density on the aqueous solubility of quartz and some geological implications: a theoretical approach. *J Geophys Res* 90:3649–3657
- Wolff E (1845) Chemisch-mineralogische Notizen 3: über den Glühverlust des Quarzes und des Feldspaths. *J Pract Chem* 34:1–237
- Yund RA, Smith BM, Tullis J (1981) Dislocation-assisted diffusion of oxygen in albite. *Phys Chem Miner* 7:185–189

Editorial responsibility: J. Touret